ACS APPLIED MATERIALS & INTERFACES

Research Article

www.acsami.org

Gracilaria lemaneiformis Polysaccharide as Integrin-Targeting Surface Decorator of Selenium Nanoparticles to Achieve Enhanced Anticancer Efficacy

Wenting Jiang,[†] Yuanting Fu,[†] Fang Yang,*[,†] Yufeng Yang,[‡] Ting Liu,[†] Wenjie Zheng,*[,†] Lilan Zeng,[†] and Tianfeng Chen*[,†]

[†]Department of Chemistry and [‡]Institute of Hydrobiology, College of Life Science and Technology, Jinan University, Guangzhou 510632, China

Supporting Information

ABSTRACT: The poor permeability of glioma parenchyma represents a major limit for antiglioblastoma drug delivery. *Gracilaria lemaneiformis* polysaccharide (GLP), which has a high binding affinity to $\alpha_v\beta_3$ integrin overexpressed in glioma cells, was employed in the present study to functionalize selenium nanoparticles (SeNPs) to achieve antiglioblastoma efficacy. GLP−SeNPs showed satisfactory size distribution, high stability, and selectivity between cancer and normal cells. In U87 glioma cell membrane, which has a high integrin expression level, GLP−SeNPs exhibited significantly higher cellular uptake than unmodified SeNPs. As expected, U87 cells exhibited a greater uptake of GLP−SeNPs than C6 cells with low integrin expression level. Furthermore, the internalization of GLP−SeNPs was inhibited by cyclo-(Arg-Gly-Asp-Phe-Lys) peptides, suggesting that cellular uptake into U87 cells and C6 cells occurred via $\alpha_v\beta_3$ integrin-mediated endocytosis. For U87 cells, the cytotoxicity of SeNPs decorated by GLP was enhanced significantly because of the induction of various apoptosis signaling pathways. Internalized GLP−SeNPs triggered intracellular reactive oxygen species downregulation. Therefore, p53, MAPKs, and AKT pathways were activated to advance cell apoptosis. These findings suggest that surface decoration of nanomaterials with GLP could be an efficient strategy for design and preparation of glioblastoma targeting nanodrugs.

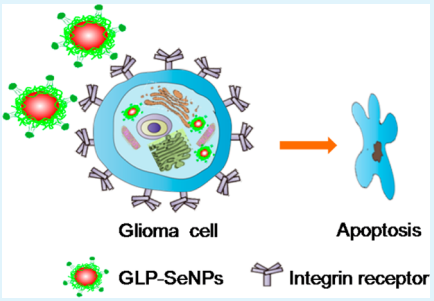

KEYWORDS: *cancer targeting, glioblastoma, selenium nanoparticles, polysaccharide, apoptosis*

INTRODUCTION

Glioblastoma multiforme (GBM) is becoming the most lethal primary brain tumor in humans worldwide, representing approximately 45−50% of all primary intracranial tumors. Malignant gliomas are typically extremely aggressive, highly invasive, and neurologically destructive tumors. Malignant gliomas are locally invasive tumors that are unpredictable and the nodus of treatment at present. Consequently, patients diagnosed with malignant gliomas have only a very poor survival rate.[1−3] Therefore, great efforts have been paid to explore effective therapeutic modalities for antiglioblastoma therapy. Glioma cells are widely distributed throughout the brain and have no obvious boundary from other brain normal cells. Therefore, it is very difficult to make a complete surgical resection. Moreover, GBM has a high recurrence rate and a high mortality rate.[4] Other treatment methods such as radiotherapy or chemotherapy followed by surgery resection are also essential in the treatment of malignant gliomas. For example, biodegrable carmustine wafers improved the total life expectancy of cancer patients;[5] however, their benefits are limited due to the deficiency in drug accumulation in the glioma and the substantial side effects generated by nonspecific biodistribution.[6−8] Unfortunately, most of the chemotherapeutic agents failed to step over the blood−brain barrier (BBB) and blood−tumor barrier (BTB), which restricts the drugs from reaching the glioma sites. Therefore, it causes low penetration across the BBB and poor action efficacy of the chemotherapeutics.[9−11] Accordingly, in order to overcome the BBB and BTB restrictions, multifunctional drug delivery systems based on cell membrane receptor-mediated targeting cellular uptake have kindled great interest of scientists involved in antiglioblastoma therapy.[12]

Nanobiotechnology, especially nanoparticles with good biocompatibility and targetability, is playing an increasingly significant role in enhancement of drug uptake in cancer cells, and these nanobiotechnology can be applied to treatments of glioma.[13] Selenium (Se) is a vital dietary trace element and necessary for mammalian life. It plays an essential role in the growth and functioning of living cells of higher animals and humans. Lack of Se will lead to damage of the immune system and increase the risk of developing cancers.[14] Recently, a novel Se species, elemental Se nanoparticles (SeNPs), has attracted more and more attention for their higher anticancer efficacy and lower side effects compared to other inorganic and organic

Received: May 22, 2014
Accepted: July 29, 2014
Published: July 29, 2014

selenocompounds.[15] Many studies have shown that SeNPs exhibited excellent antioxidant activities in vitro and in vivo through improved activation of selenoenzymes that delete free radicals inside the body.[16] Nevertheless, SeNPs without specific cell targeting effects may results in drug toxicity and adverse side effects to cancer patients. Furthermore, development of SeNPs as an anticancer agent has been difficult due to the poor stability and low cellular accumulation.[17] Therefore, an effective cancer-targeting design could enhance the drug delivery system. Particularly, cancer-targeted ligands could be linked to nanoparticles through covalently or noncovalently bonds. This could enhance the ability of nanoparticles to specifically accumulated in cancer cells but not in normal cells..

In recent decades, natural polysaccharides as unique raw materials have been attracting particular interest for the attractive characteristics, such as nontoxicity, high compatibility and degradability, hydrophilicity, and protectiveness, which are pivotal characteristics for pharmic delivery and interception.[18−20] The majority of polysaccharides have the effects of antivirus, anticancer, and immune-enhancing activities. For example, a lot of derivatives of chitosan could enhance drug uptake in cells and increase gene expression as a nonviral vector.[21−23] In addition, spirulina polysaccharide (SPS) is also found as an effective inhibitor of corneal neovascularization; thus, it exhibits application potential in therapy of corneal diseases involving neovascularization and inflammation.[24] *Gracilaria lemaneiformis*, phylum Rhodophyta, family Gracilariaceae, and genus *Gracilaria*, possesses many bioactive functions such as antitumor, antiviral, antioxidant, hypotensive, and hypolipidemic effects.[25] Polysaccharide is the key component and important biological active substance of *G. lemaneiformis*. D-Galactose and 3,6-anhydro-L-galactose are basic units of *G. lemaneiformis* polysaccharide (GLP).[26] It has been reported that $\alpha_v\beta_3$ integrin is an important receptor of cellular adhesion molecules, which is overexpressed in the majority of maglignant tumors such as glioma, melanoma, ovarian, and breast cancers.[27] In this study, GLP exhibits a fairly high affinity to $\alpha_v\beta_3$ integrin. GLP extracted from the alga *G. lemaneiformis* can be degraded by hydrogen peroxide (H_2O_2). After degradation, the biological activity of GLP can be noticeably improved.[28] Thus, GLP could serve as an ideal candidate for therapeutics of cancers. In this study, GLP was used as a surface decorator of nanomaterials. SeNPs functionalized by GLP (GLP−SeNPs) were prepared in an attempt to increase the retention time of Se, thus achieving higher cellular uptake and improved cancer-targeting effects and anticancer efficacy. GLP and SeNPs were coadministered to enhance glioblastoma-specific drug accumulation and penetration. The in vitro antiglioblastoma effects and the underlying action mechanisms were investigated in detail. Taken together, our results suggest that GLP could be an ideal surface decorator for nanomaterials in design and construction of glioblastoma-targeting nanodrugs.

EXPERIMENTAL METHODS

Materials. Polysaccharide powder of GLP was provided by the Institute of Hydrobiology, Jinan University. Caspase substrates were purchased from Calbiochem. The chemical reagents were purchased from Sigma−Aldrich. Milli-Q water used in this study was collected from a ultrapure water purification system (Millipore).

Preparation of GLP and GLP−SeNPs. GLP solution was prepared via an oxidative degradation technique as described.[28] Briefly, 0.5 g of GLP was dissolved into 50 mL of Milli-Q water to form a 1% mixed solution, 1 mL of 30% H_2O_2 was added, and the solution was ultrasonicated by using a water bath at 65 °C for 6 h at 100 W. Then, the reaction solution was filtered, and the precipitate was washed with Milli-Q water. Finally, the precipitate was diluted with Milli-Q water to 50 mL. Four samples were prepared, and the concentrations of GLP were 0.2, 1, 5, and 10 mg/mL, respectively. Samples were stored at 4 °C.

Se nanoparticles were prepared utilizing the same method as previously described.[29,30] Fresh Na_2SeO_3 and ascorbic acid (Vc) solutions of 100 mM concentration were prepared. At room temperature, the Na_2SeO_3 solution was added into the different mass concentrations of GLP solutions, and the final concentration of Na_2SeO_3 was 2 mM. Then, Vc was added drop by drop to the mixture, and the four mixtures were stirred for 24 h on a magnetic stirring apparatus. The excess GLP and Na_2SeO_3 were eliminated by dialysis for 24 h. Inductively coupled plasma−atomic emission spectroscopy was applied to determine the Se concentrations. The in vitro cellular uptake and localization of GLP−SeNPs were determined by using coumarin-6, which was incorporated into GLP−SeNPs and acted as a probe. The 4 μg/mL coumarin-6 was prepared with the same procedure except being added into the Na_2SeO_3 and GLP solution before Vc to form coumarin-6-loaded GLP−SeNPs.

Characterization of GLP−SeNPs. Transmission electron microscopy (TEM, Hitachi, H-7650) was used to characterize the obtained GLP−SeNPs. According to the TEM protocol, the power particles were dispersed onto a holey carbon film on copper grids, and then, micrographs were recorded at an acceleration voltage of 80 kV. A Zetasizer Nano ZS particle analyzer (Malvern Instruments Limited) was used to determine the size hydrodynamic distribution and stability of the nanoparticles in aqueous solution. Fourier transform infrared spectroscopy (FT-IR, Equinox 55, Bruker) was measured in the range 4000−500 cm^{-1}.

Hemolysis Activity Examinations. The hemolysis property of GLP−SeNPs was examined by spectrophotometry as in Nogueira et al.[31] The erythrocyte agglutination of samples was studied by a phase contrast microscope (Life technologies, EVOS FL auto) for 10 or 120 min (SeNPs, GLP, and GLP−SeNPs at concentrations of 5, 10, and 20 μM).

Cell Culture and Cell Viability by MTT Assay. All human cell lines were gliocytoma cells in this study, including U87 and C6 cells. Chem-5 cells (human brain glial cells), HK-2 (Human Glandular Kallikrein-2), L02 human liver cells, HepG-2 cells (liver hepatocellular cells), Hela cells (Henrietta Lacks strain of cancer cells), MCF-7 cells (Michigan Cancer Foundation-7 cells), and A375 cells (human-melanoma cell line A375) were purchased from American Type Culture Collection (ATCC, Manassas, VA, USA). As described in our previous papers,[30] in a humidified incubator with 5% CO_2 atmosphere, all cell lines were incubated in DMEM media supplemented with 10% fetal bovine serum, 50 units/mL streptomycin and 100 units/mL penicillin at 37 °C. Cell viability was determined by MTT assay according to the protocol.[29] GLP−SeNPs with different concentrations were added into cells that were already seeded in culture plates for 24 h at 37 °C. After 72 h, MTT solution (5 mg/mL in PBS, 20 mL) was added. The medium containing MTT was removed after 5 h, and DMSO (150 mL) was added. Finally, by using a microplate spectrophotometer (Versamax) and with DMSO as the blank, the absorbance at 570 nm was recorded. The data were expressed as the percentage of MTT reduction relative to the absorbance of control cells. In addition, the cell viability of U87 cells or C6 cells was determined in the same way after they were treated with different concentrations of GLP−SeNPs for 24, 48, and 72 h.

Cellular Uptake Mechanisms of GLP−SeNPs. Quantitative analysis of cellular uptake of GLP−SeNPs was carried out by using a fluorescence microplate reader as described in our previous papers.[32] With excitation and emission wavelengths at 430 and 485 nm, fluorescence intensity from 6-coumarin-loaded GLP−SeNPs inside the wells was recorded. The percentage of the fluorescence of the nanoparticles over that added was the cellular uptake efficiency.

Furthermore, U87 cells and C6 cells were also seeded and incubated with a density of 8000 cells per well (100 μL). After 24 h, the medium was removed and changed into cyclo-(Arg-Gly-Asp-Phe-Lys) (cRGDfK) peptide (2 mg of cRGDfK peptide was dissolved into

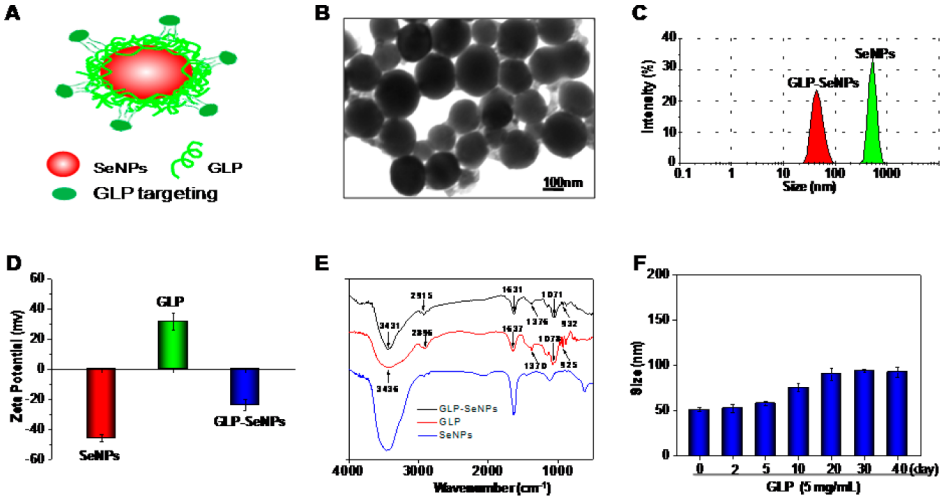

Figure 1. Characterization of GLP−SeNPs. (A) Schematic structure of GLP−SeNPs. (B) TEM images of GLP−SeNPs (5 mg/mL GLP), scale bar 100 nm. (C) Size distribution of SeNPs and GLP−SeNPs (5 mg/mL GLP). (D) ζ potentials of SeNPs, GLP, and GLP−SeNPs (5 mg/mL GLP). (E) FT-IR spectra of SeNPs, GLP, and GLP−SeNPs (5 mg/mL GLP). (F) Time course of size distribution of GLP−SeNPs (5 mg/mL GLP).

700 μL of PBS and diluted into different concentrations). After 2 h of incubation, the same concentration of 6-coumarin-loaded GLP−SeNPs was added. Finally, after 4 h of incubation, the cellular uptake efficiency was determined by fluorescence microplate.

Intracellular Trafficking of GLP−SeNPs. The lysosomal marker Lyso Tracker Red was used to trace the intracellular localization of coumarin-6-loaded GLP−SeNPs in U87 cells. First, U87 cells were incubated in 2 cm cell culture dishes with 80 nM lyso-tracker DND-99 (Sigma−Aldrich) for 2 h until 70% confluence was stained. Then, 1 mg/mL DAPI H33258 (Sigma−Aldrich) was added. After 30 min, 160 μM 6-coumarin-loaded GLP−SeNPs and Lyso Tracker Red were incubated for different times at 37 °C. After rinsing them with PBS for three times, the stained cells were examined by using a fluorescence microscope (Nikon Eclipse 230 80i).

Flow Cytometric Analysis. Flow cytometry was carried out as described in our previous study.[30] By using MultiCycle software, we analyzed the cell cycle distribution. The proportion of the cells in G0/G1, S, and G2/M phases was expressed as a DNA histogram. The apoptotic cells with hypodiploid DNA contents were detected by quantifying the sub-G1 peak.

Caspase Activity. As described in our previous paper, with the excitation and emission wavelengths at 380 and 460 nm, respectively, caspase activity was determined by fluorescence intensity with using specific caspase-3, -8, and -9 substrates.[17]

Intracellular Reactive Oxygen Species (ROS) Generation. GLP−SeNPs induced ROS were analyzed as previously described.[17] After the cells were stained with dihydroethidium (DHE, Beyotime), utilizing a fluorescence microplate reader, with excitation and emission wavelengths at 300 and 600 nm, respectively, the intracellular ROS was monitored by analyzing the DHE fluorescence intensity.

Western Blot. Total cellular proteins were acquired after U87 cells were treated with GLP−SeNPs for 72 h and incubated with lysis buffer (Beyotime). Then, the effects of GLP−SeNPs on the expression levels of proteins associated with different signaling pathways were analyzed.[17]

Statistical Analysis. Results were expressed as the mean ± standard deviation (SD), which were from at least three independent experiments. A two-tailed Student's *t* test was applied to analyze the difference between two groups. One-way ANOVA multiple comparisons were used to analyze the significance among three or more groups. Difference with $P < 0.05$(*) or $P < 0.01$(**) was considered statistically significant.

RESULTS AND DISCUSSION

Design and Characterization of GLP−SeNPs. Most of the natural polysaccharides reported possess a variety of biological activities. The most attractive characteristic of these polysaccharides is their antitumor activities, and they can be used as a decorator to stabilize inorganic nanomaterials.[29] GLP, extracted from *G. lemaneiformis*, is a natural polysaccharide complex. GLP possesses anticancer activity, but degraded GLP has demonstrated higher anticancer activities.[28] In this study, GLP was attached to SeNPs as a capping agent, so that the targeting effects and cell-penetrating activity of SeNPs were significantly improved. It was reported that Se nanoparticles can be produced by the redox reaction between selenite and ascorbic acid.[29,32] Therefore, Se nanoparticles were obtained in the same way in our study. According to the previous study, D-galactose and 3,6-anhydro-L-galactose are the major components of GLP, and there are a large number of hydroxyl groups and amino groups in GLP.[33] Therefore, stable and size-controllable GLP−SeNPs were successfully obtained by attaching GLP to the surface of SeNPs (Figure 1A). SeNPs were very unstable when there was no GLP. The precipitation−accumulation course of SeNPs was very rapid. However, the solution of GLP−SeNPs was monodispersed when GLP existed. In addition, the average diameter of GLP−SeNPs was the minimum with an average diameter of 50 nm when the GLP concentration was 5 mg/mL. The average diameter reached 600 nm without GLP surface decoration (Figure 1C) because of the fast precipitation and accumulation of SeNPs. Moreover, the particle size of GLP−SeNPs could be regulated (Figure S1, Supporting Information). The particle size exceeded 50 nm when GLP concentration was 0.2 or 1 mg/mL, and the diameter of GLP−SeNPs was about 123 nm when the concentration of GLP was 10 mg/mL. Results indicated that GLP regulated the particle size of SeNPs effectively in a specific range of concentrations. The stability of nanoparticles is an important indicator in measuring its application prospect. When the concentration of GLP−SeNPs was 5 mg/mL, the particle size of GLP−SeNPs showed a slight increase as the storage time increased, but the size remained within 100 nm in 40 days (Figure 1F), which was more stable than that of SeNPs decorated by mushroom polysaccharides−protein complexes

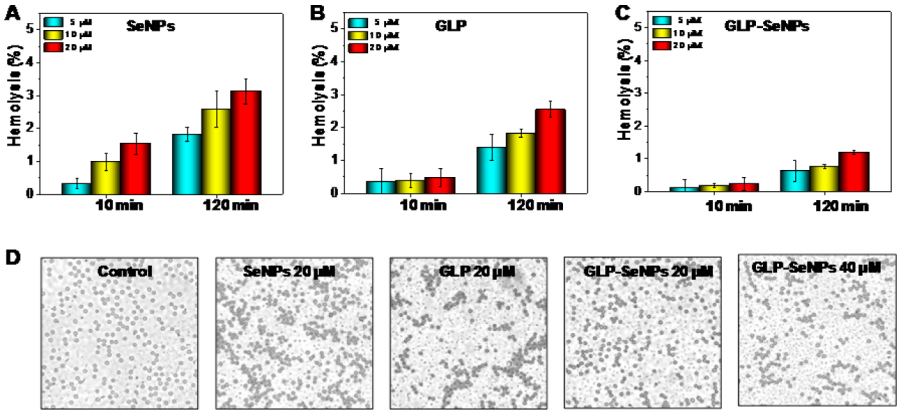

Figure 2. Hemocompatibility of SeNPs, GLP, and GLP−SeNPs. (A−C) Percentage of hemolysis caused by SeNPs, GLP, and GLP−SeNPs after incubation with human erythrocytes for 10 and 120 min at 37 °C, respectively. Each value represents the mean ± SD of three experiments. (D) Human erythrocytes agglutination investigated by phase microscopy after incubation with SeNPs, GLP, and GLP−SeNPs for 2 h, respectively.

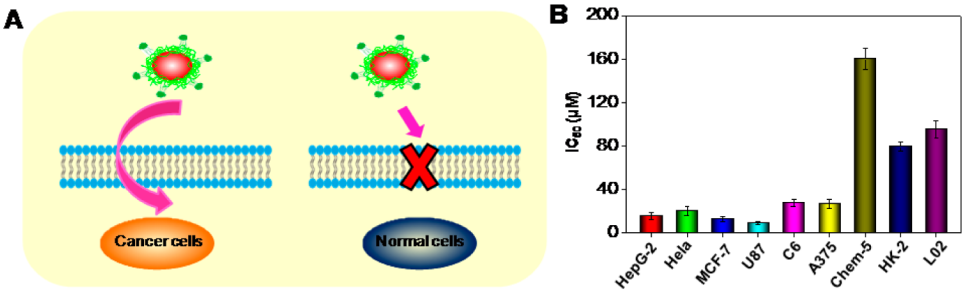

Figure 3. (A) Scheme of GLP−SeNPs targeting effects on cancer cells. (B) Antitumor activity of GLP−SeNPs on various glioma cells and normal cells. Each value represents means ± SD (n = 3).

within the same period of time.[29] Besides, as shown in Figure 2D, the ζ potentials of SeNPs, GLP, and GLP−SeNPs were −45.8, 31.6, and −24.0 mV, respectively. The differences in ζ potential, demonstrating the adsorption between SeNPs and GLP, was mainly controlled by electrostatic forces.

The TEM image showed that GLP−SeNPs were monodisperse particles with high uniformity in water and near-spherical in shape. Similarly, as shown in Figure 1B, the size determined by TEM was consistent with those previously measured. Figure 1E showed the FT-IR spectra of SeNPs, GLP, and GLP−SeNPs, respectively. The resemblance of three spectra indicated that SeNPs and GLP formed the GLP−SeNPs. In all three spectra, the characteristic absorption peaks of the hydroxyl group (−OH) were observed. However, the peak in the GLP spectrum at 3436 cm^{-1} shifted slightly to 3431 cm^{-1} in the GLP−SeNPs spectrum, indicating the weak interaction between the hydroxyl group and Se atoms. The peak at 1637 cm^{-1} corresponded to the stretching vibration of −CO−NH− in the GLP spectrum shifted to 1631 cm^{-1} in the GLP−SeNPs spectrum. The above results suggested that Se−O and Se−N bonds might be formed between SeNPs and GLP. Moreover, the IR O═S═O asymmetric stretching vibration absorbance peaks at 1376^{-1} cm in the spectrum of GLP−SeNPs indicated the existence of a sulfated group. Additionally, the characteristic absorption peak at 932 cm^{-1} was assigned to 3,6-anhydro-galactose, the intense peak at 1071 cm^{-1} was attributed to the glycosidic linkage C−O−H and C−O−C stretching vibration, and the weak peak at 2915 cm^{-1} corresponded to the C−H stretching vibration.[33] The difference and appearance of the above peaks from the IR spectra indicated the surface decoration of SeNPs by GLP, which could contribute to the high stability of the nanoparticles.

Hemocompatibility of GLP−SeNPs. The hemolysis experiments were performed to study the hemocompatibility of the nanoparticles (Figure 2). The hemolysis test is considered as a very simple and indispensable measure to assess the hemocompatibility of materials.[34] The release of hemoglobin was used to quantify their erythrocyte-damaging properties.[31] The red blood cells (RBCs) were exposed to SeNPs and GLP−SeNPs at different concentrations for 10 and 120 min, respectively. As shown in Figure 2A−C, the nanoparticles showed minor hemolysis destruction (less than 5%) to RBCs even at a high concentration of 20 μM. The hemolysis rate of GLP−SeNPs was lower (less than 1.5% even at the highest concentration) than the unloaded SeNPs and single GLP in all conditions. Similarly, as shown in Figure 2D, slight agglutination of erythrocytes was induced by 20 μM concentration of unloaded SeNPs and GLP, but there was no agglutination after treatment with 20 μM GLP−SeNPs for 2 h. Only a few gathered until treated with 40 μM GLP−SeNPs. These results indicated that SeNPs, GLP, and GLP−SeNPs were hemocompatible allowing potential application for drug delivery but GLP−SeNPs was much better than unloaded SeNPs and single GLP in their delivery efficiency. There is some evidence that the properties of nanoparticles such as structure, size, surface chemistry, softness, surface charge, and agglomeration state play an important role in the interaction with RBCs.[35] Therefore, the main reason for the low hemolysis rate might be that the nanoparticles were hydrophilic and had a small size.

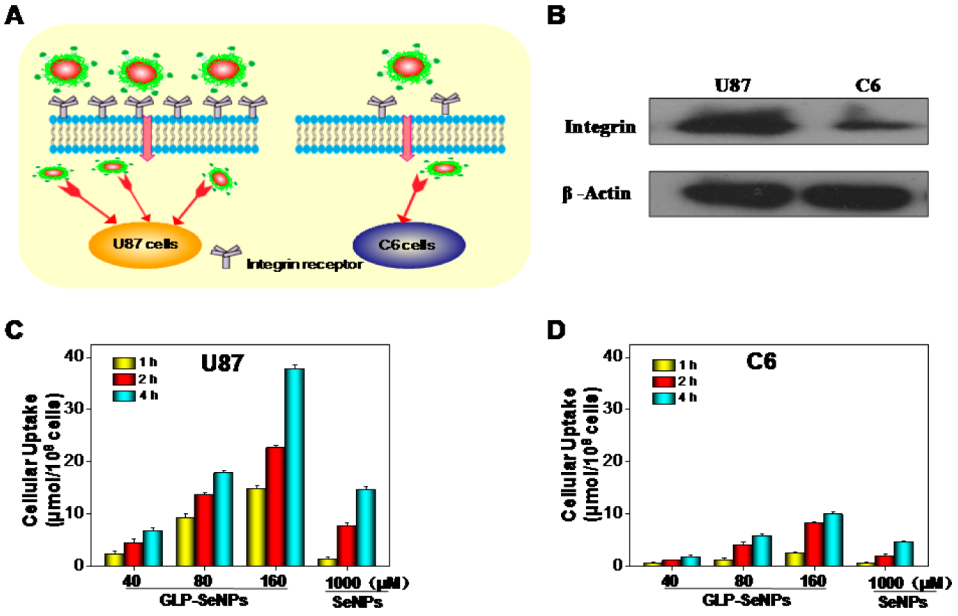

Figure 4. Selective cellular uptake of GLP−SeNPs. (A) Scheme of GLP−SeNPs targeting effects on U87 cells and C6 cells. (B) Integrin expression in U87 and C6 cells. Western blot was applied to determine the expression level of integrin. (C) Quantitative analysis of cellular uptake efficacy of coumarin-6-loaded GLP−SeNPs in U87 cells. (D) Quantitative analysis of cellular uptake efficacy of coumarin-6-loaded GLP−SeNPs in C6 cells. Each value represents means ± SD (n = 3).

In Vitro Anticancer Activity of GLP−SeNPs. In the preliminary screening, nine cell lines were treated with the GLP−SeNPs. HepG-2, Hela, MCF-7, U87, C6, and A375 cells are the most common malignant tumor cells. Chem-5, HK-2, and L02 cells were human normal cells. The results indicated that GLP−SeNPs were more cytotoxic to the tumor cells than human normal cells (Figure 3A). Moreover, the GLP−SeNPs were most sensitive to U87 cells with an IC_{50} value of 9.1 ± 1.53 μM and significantly inhibited the U87 cells growth in a dose-dependent manner as shown in Figure 3B. However, the GLP−SeNPs were noncytotoxic toward the normal brain glial cells (Chem-5: IC_{50} = 159.9 ± 9.73 μM), Hk-2 cells (human kideny cell: IC_{50} = 79.5 ± 4.26 μM), and L02 cells (human liver cell: IC_{50} = 95.6 ± 7.68 μM). The results idicated the low cytotoxicity of GLP−SeNPs to normal human cells and their cytotoxicity was cancer specific. Moreover, C6 cells also belong to the gliomas, and the IC_{50} value was 27.6 ± 3.13 μM. Therefore, the most sensitive U87 cells and C6 cells were chosen to further elucidate the aiticancer action of GLP−SeNPs. The different sensitivity of cancer cells to GLP−SeNPs could be due to their diversified cellular protein expression profiles.

The cell viability of GLP−SeNPs, SeNPs, and GLP on U87 cells and C6 cells was also analyzed (Figure S2, Supporting Information). It demonstrated low toxicity to U87 cells and C6 cells when SeNPs or GLP was provided alone. Only GLP−SeNPs could significantly affect the cell viability and had a higher effect on U87 cells than C6 cells. Furthermore, the cell viability was determined by GLP−SeNPs at 24, 48, and 72 h (Figure S3, Supporting Information). After exposure to GLP−SeNPs for different times, the growth of U87 and C6 cell lines was obviously inhibited, but the viability of U87 cells was lower than that of C6 cells in a dose- and time-dependent manner. For example, the cell viability of U87 cells was 44.6% after treatment with 10 μM GLP−SeNPs for 72 h, which was lower than that of C6 cells at 68.5%. Likewise, when the cell viability of U87 and C6 cells was 50.0% in 72 h, the IC_{50} value of U87 cells was 8.62 μM, which was lower than that of C6 cells at 24.11 μM. The results indicated that the GLP−SeNPs exhibited higher cytotoxicity against U87 cells than C6 cells under the same conditions.

In Vitro Cellular Uptake of GLP−SeNPs. The efficacy of cellular uptake is an important parameter for delivering the targeted nanomaterial-based drug successfully.[36] In this study, GLP on the surface of SeNPs identified the overexpressed integrin receptor in the glioma cell membrane, which effectively enhanced the cellular uptake of tumor-targeting nanoparticles (Figure 4A). Recently, it was reported that the expression level of $\alpha_v\beta_3$ integrin in U87 cells is much higher than in C6 cells.[37] Therefore, the expression level of the integrin receptor on the cell membrane should be examined first in order to analyze whether the receptor contributes to the cellular uptake of GLP−SeNPs. The results indicated that the expression level of integrin receptor was obviously higher in U87 cells compared to C6 cells (Figure 4B), suggesting that GLP had a superior guided selectivity for U87 cells to C6 cells.

The quantitative analysis of cellular uptake, which confirmed the dose-dependent cellular association of GLP−SeNPs and SeNPs in U87 and C6 cells, was carried out by analyzing fluorescence intensity from intracellular coumarin-6-loaded nanoparticles.[29] Before analyzing fluorescence intensity, U87 and C6 cells were first incubated with 40, 80, and 160 μM coumarin-6-loaded GLP−SeNPs and 1000 μM coumarin-6-loaded SeNPs for 1, 2, and 4 h. Results are shown in Figure 4C, D. The intracellular concentrations of GLP−SeNPs increased in a time- and dose-dependent manner. A higher accumulation of GLP−SeNPs was observed compared with that of SeNPs in U87 cells than in C6 cells. After 1, 2, and 4 h incubations with 160 μM 6-coumarin-loaded GLP−SeNPs, the GLP−SeNPs intracellular concentrations increased from 14.5 to 22.6 and 37.7 μmol per 10^8 cells, respectively, which were several times higher than 1000 μM SeNPs without GLP surface decoration in U87 cells. However, the absorption efficiency was lower regardless if GLP−SeNPs or SeNPs were added in C6 cells.

Therefore, these results demonstrated that the uptake and cytotoxicity of SeNPs against cancer cells could be efficiently improved by GLP decoration, which is similar to chitosan as previously reported.[38]

Fluorescent microscopy analysis showed the intracellular trafficking of GLP−SeNPs in U87 cells, so the intracellular trafficking of coumarin-6-labeled GLP−SeNPs in U87 cells was observed. Lyso Tracker Red was used to label lysosomes, and DAPI is a blue nuclei dye. As shown in Figure 5, after 1 h exposure to coumarin-6-labeled GLP−SeNPs, the cellular-associated fluorescent signal in U87 cells was observed, indicating that GLP−SeNPs shuttled across the cell membrane in 1 h accumulated gradually in lysosomes and eventually dispersed in the cytoplasm. After incubated for 8 h, we observed a higher accumulation of GLP−SeNPs with bright fluorescence. During the whole experimental process, no green fluorescence signal was detected in the blue cell nucleus; therefore, the main target of GLP−SeNPs is the lysosome rather than the nucleus.

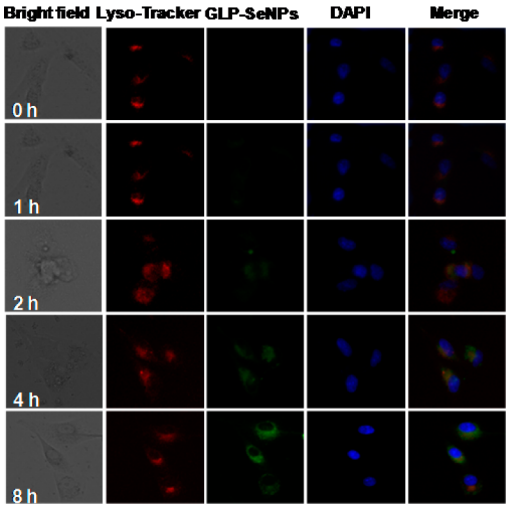

Figure 5. Intracellular trafficking of coumarin-6-loaded GLP−SeNPs in U87 cells. The cells were treated with coumarin-6-loaded GLP−SeNPs (160 μM) for different periods of time and stained with lysotracker (red fluorescence, lysosome) and DAPI (blue fluorescence, nucleus). Original magnification: 20×.

In order to further investigate the importance of the integrin receptor, a cRGDfK peptide competing assay was performed. To study whether GLP could guide conjugate GLP−SeNPs to $\alpha_v\beta_3$ integrin-rich tumor cells, cRGDfk peptide were preincubated with U87 and C6 cells for 2 h and then treated with GLP−SeNPs (160 μM). As shown in Figure 6, the cellular association of GLP−SeNPs was remarkably inhibited by preadded cRGDfk in a dose-dependent manner. cRGDfk effectively blocked the internalization of GLP−SeNPs in U87 and C6 cells. Likewise, the cellular uptake in U87 cells was greater than in C6 cells no matter what the concentration of cRGDfk peptide was. These expected results demonstrated that $\alpha_v\beta_3$ integrin receptor-mediated endocytosis might explain the selective cellular uptake of GLP−SeNPs between U87 and C6 cells.

Induction of Cancer Cell Apoptosis by GLP−SeNPs. Apoptosis plays an essential role in a wide variety of different biological systems, including normal cell cycle, the immune system, embryonic development, morphologic change, and chemical-induced cell death.[39] Moreover, cell apoptosis was postulated to be the crucial mechanism for the anticancer activity of Se and selenocompounds.[40] To investigate whether apoptosis was involved in cell death induced by GLP−SeNPs, flow cytometry was performed. As the results show in Figure 7, a significant dose-dependent increase in sub-G1 cell amount was observed after U87 and C6 cells were treated with GLP−SeNPs for 72 h, and the cell population of sub-G1 phase determined the ultimate degree of cell apoptosis. When treated with the same concentration of GLP−SeNPs (20 μM), the U87 cell population of sub-G1 peaks was 41.6%, which was much higher than the impact on C6 cells (8.1%). Only 12.4% C6 cell number of sub-G1 peaks was observed when the concentration of GLP−SeNPs reached 80 μM. No significant change was detected in G0/G1, S, and G2/M phases.

Caspases are a family of cystein proteases, and they are very important during apoptosis.[41] Caspase-3 plays a pivotal role in diseases related cell apoptosis,[42] while caspase-8 and -9 play the part of initiators of death receptor-mediated and mitochondria-mediated apoptotic pathways, respectively.[43] To identify how caspases are involved in GLP−SeNPs-induced apoptosis, a fluorometric assay was applied to measure the activation of caspase-8, caspase-9, and caspase-3. The results elucidated that GLP−SeNPs triggered dose-dependent activation of caspase-3, caspase-8, and caspase-9 in U87 and C6 cells (Figure 8A, B), which indicated that both of the pathways, death receptor-mediated and mitochondria-mediated pathways, were involved in the apoptosis induced by GLP−SeNP. It could be observed that, no matter in U87 or C6 cells, the activity of caspase-9 had a markedly higher level compared to caspase-8. The GLP−SeNPs played a higher impact on U87 cells than C6 cells once again. A western blotting assay was taken to further study the expression level of caspases in U87 cells after being treated with different concentrations of GLP−SeNPs. Poly-ADP−ribose

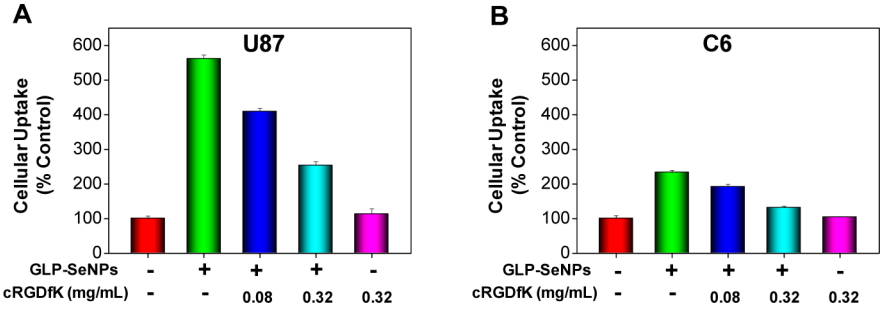

Figure 6. (A, B) Effects of cRGDfK peptide on the cellular internalization induced by GLP−SeNPs. The cells were exposed to cRGDfK peptide for 2 h and then treated with GLP−SeNPs (160 μM) for 1 h. All experiments were performed in triplicate.

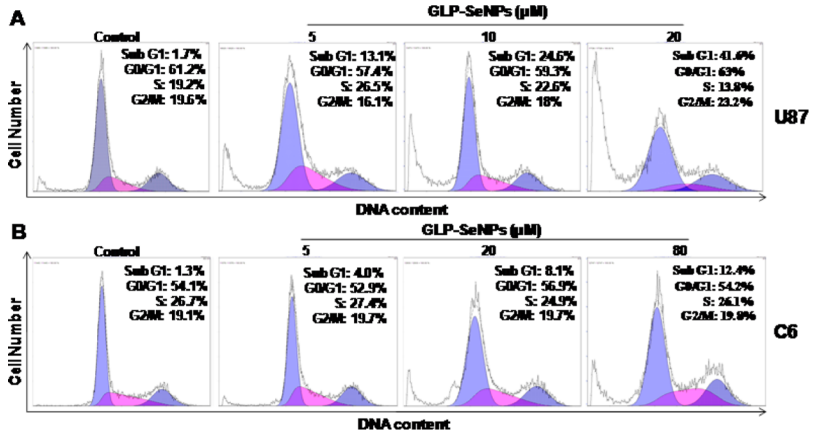

Figure 7. Flow cytometry of (A) U87 and (B) C6 cells treated with GLP−SeNPs for 72 h.

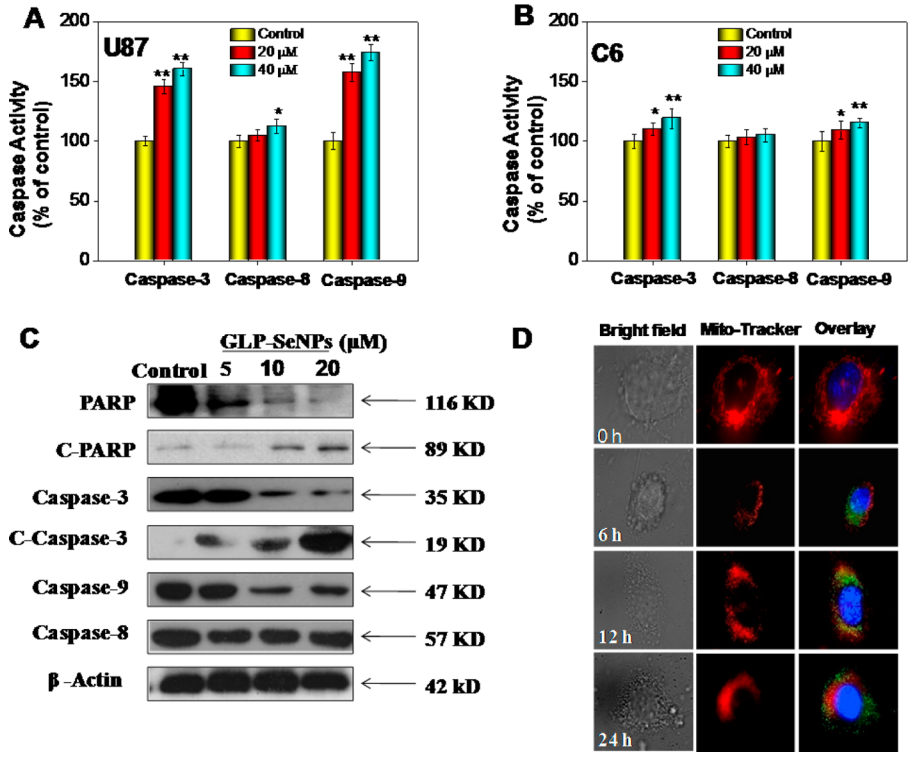

Figure 8. Caspase activity in GLP−SeNPs-induced apoptosis in (A) U87 and (B) C6 cells. U87 and C6 cells were exposed to GLP−SeNPs for 72 h. Difference between groups is indicated at $*P < 0.05$ and $**P < 0.01$. (C) The expression of caspase family members by western blot. β-Actin was used as loading control. (D) Colocalization of GLP−SeNPs (green fluorescence), DAPI (blue fluorescence), and mito-tracker (red fluorescence) in U87 cells. Original magnification: 100×.

polymerase (PARP) is a DNA repairase and induces cell apoptosis. PARP is also the cleavage substrate of caspase in cell apoptosis.[44] As shown in Figure 8C, the expression level of caspase-3, -8, -9, and PARP were downregulated with rise in concentration. On the contrary, the expression level of c-PARP and c-caspase-3 were on the rise. Therefore, after treated with GLP−SeNPs for 72 h, caspase-3, -8, and -9 could be activated effectively and triggered cleavage PARP in U87 cells.

Mitochondria are the energy factories of cellular activities, but a variety of factors can result in damage to the structure and function of mitochondria and further induce cell apoptosis.[45] We also investigated whether GLP−SeNPs had any impact on mitochondria. Fluorescent microscopy imaging was used to analyze nanoparticles in U87 cells. As shown in Figure 8D, two special fluorescent tracers, red mito-tracker and blue DAPI, were used to label the mitochondria and the nucleus. At first, mitochondria were present as red threadlike filaments; then, U87 cells treated with 6-coumarin−GLP−SeNPs (green fluorescence) entered into the cytoplasm and finally dispersed around the mitochondria. We observed mitochondria fragmentation and aggregation, and at 24 h, they came together into small particles. The results suggested that GLP−SeNPs also had an impact on mitochondria.

Activation Intracellular Apoptotic Signaling Pathways by GLP−SeNPs. The intermediate level ROS is a crucial factor in all kinds of cell signal ways. ROS concentration can cause cell damage and even induce cell apoptosis.[46] In order to study whether GLP−SeNPs could trigger ROS-mediated apoptosis,

the intracellular ROS level was monitored by detecting the fluorescence intensity of dihydroethidium. As shown in Figure 9A, ROS generation of U87 cells declined sharply after the exposure to GLP−SeNPs at different concentrations for 10 min, which did not change in 120 min. Likewise, we observed GLP−SeNPs downregulate ROS generation (55.87%, 160 μM) in U87 cells, which was higher than that in C6 cells (27.62%, 160 μM) (Figure S4, Supporting Information) at 10 min. In order to further verify that GLP−SeNPs could induce ROS downregulation, we found the stronger fluorescent intensity of DHE in U87 cells in Figure 9B.

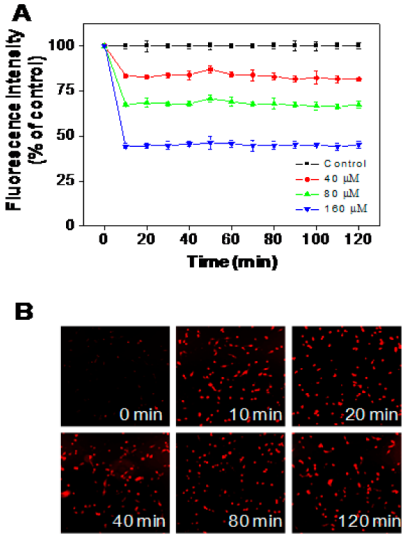

Figure 9. (A) U87 cells were treated with different concentrations of GLP−SeNPs for different times, and the intracellular ROS levels were detected by DHE fluorescence intensity. All experiments were performed in triplicate. (B) Changes of ROS level in U87 cells incubated with GLP−SeNPs for indicated times. Pictures were taken at 0, 10, 20, 40, 80, and 120 min.

Free radicals control the cellular balance between life and death by their concentrations, including cell apoptosis or necrosis. At low concentrations, ROS can activate a transcription factor and accelerate cellular proliferation and differentiation at a wider physiological significance. New research finds that ROS-mediated DNA damage can also make a difference in a series of signal transduction pathways at low concentrations, such as p-ATM, pBRCA1, pCHK1, and mitogen-activated protein kinases (MAPKs) pathways.[47]

p53, a tumor suppressor gene, acts as a transcriptional factor to affect cell cycle arrest, the DNA repairing system, and cell apoptosis.[48] The expression of p53 and its phosphorylation in U87 cells were analyzed in order to show whether the p53 pathway was involved in GLP−SeNPs-induced cell apoptosis. The western blot results showed that the total p53 expression level in U87 was barely changed by the treatment of GLP−SeNPs but the phosphorylation of p53 was dramatically upregulated. The changes in phosphorylation of ATM and Chk1 could promote phosphorylation of p53 at Ser 20 and strengthen the stability and activity of the p53 tetramerization domain (Figure 10A). To investigate how p53 was activated by GLP−SeNPs, the effects of the GLP−SeNPs on DNA were examined. p53 expression could be activated by DNA damage that acts as an irritant. Moreover, the phosphorylation of the histone at the Ser 139 residue is closely related to DNA damage, especially DNA double-stranded breaks.[48] As shown in Figure 10A, the histone phosphorylation at the Ser 139 site was remarkably triggered by GLP−SeNPs. Likewise, the changes in phosphorylation of BRCA1 occurred in response to cell cycle progression and DNA damage, suggesting that the apoptosis was triggered by GLP−SeNPs through DNA damage-mediated p53 activation.

MAPK and AKT are pivotal in the research of anticancer drugs. MAPK is one of the intricate signaling pathways in

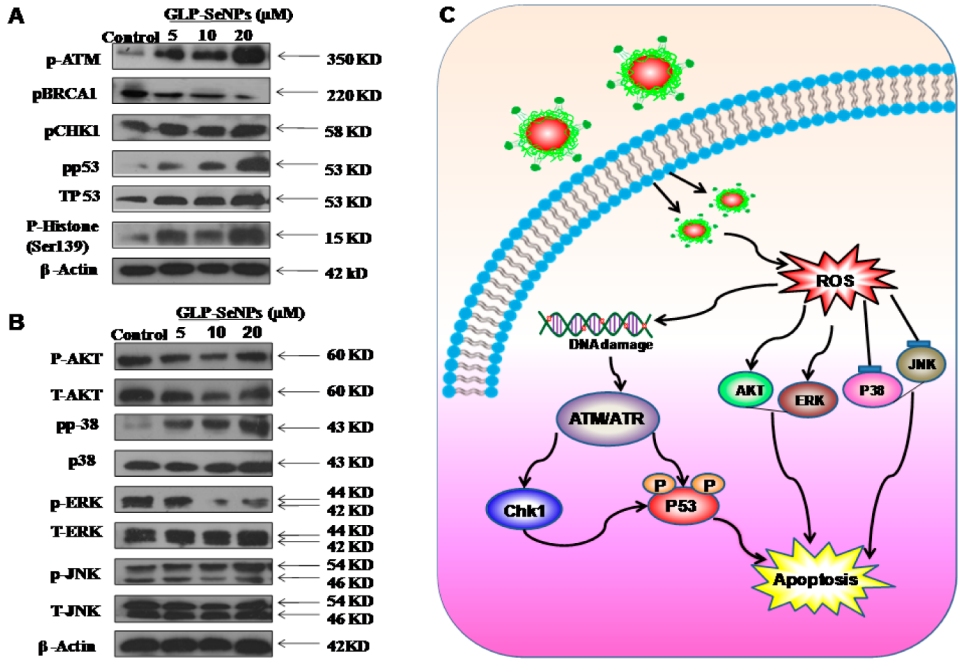

Figure 10. Activation of intracellular apoptotic signaling pathways by GLP−SeNPs in U87 cells. (A) Activation of p53 signaling pathway. (B) Phosphorylation status and expression levels of MAPKs and AKT pathways. (C) The main signaling pathway of apoptosis induced by GLP−SeNPs.

cells.[49] JNK, ERK, and P38 are all included in the family of MAPK. The MAPK cascade pathway can converge extracellular signals and play an important role in signal transduction.[50] Once the cells were treated with chemotherapeutic drugs and chemopreventive agents, the MAPK signal pathway might be activated by extracellular signal molecules and induce cell apoptosis. Moreover, AKT kinases regulate many cellular processes including cell proliferation and survival, cell size, angiogenesis, and tissue invasion.[51] After U87 cells were exposed to GLP−SeNPs, the protein expression levels of total and phosphorylated MAPKs and AKT were investigated by a western blotting assay. As shown in Figure 10B, when the U87 cells were exposed to 5, 10, and 20 μM GLP−SeNPs for 72 h, the phosphorylation of pro-apoptotic kinases p38 and JNK was upregulated in a dose-dependent trend. However, conflicting, the phosphorylation of antiapoptotic kinases AKT and ERK was remarkable repressed by GLP−SeNPs. Therefore, MAPKs and AKT signal pathways made a great contribution to apoptosis induced by GLP−SeNPs. The main signaling pathway of GLP−SeNPs-induced apoptosis is shown in Figure 10C.

CONCLUSIONS

In summary, GLP-loaded SeNPs has been successfully synthesized under a simple redox system and shown to function as an intracellular delivery system for improving anticancer activity. GLP served as a surface decorator to stabilize the SeNPs, and the size of GLP−SeNPs was controllable. GLP−SeNPs demonstrated a high selectivity between normal and cancer cells. Moreover, the cellular uptake and anticancer effect were effectively improved because of the synergism of GLP and SeNPs. The cytotoxicity toward glioblastoma was extremely enhanced by GLP−SeNPs via apoptosis induction. Furthermore, GLP−SeNPs showed a higher biological selectivity toward U87 cells than C6 cells because GLP could recognize and combine with the integrin receptor, which was overexpressed in the U87 cell membrane. From the results of in vitro anticancer activities, we concluded that GLP−SeNPs selectively infiltrated the U87 cell membrane through $\alpha_v\beta_3$ integrin-mediated uptake, which was demonstrated by preadded cRGDfk. Internalized GLP−SeNPs triggered intracellular ROS downregulation, thus accelerating cell apoptosis by activating the cell signal pathways of p53 and MAPKs. This cancer-targeted design of SeNPs that was surface decorated by GLP might provide a feasible solution for efficient antiglioblastoma drug delivery.

ASSOCIATED CONTENT

Supporting Information

GLP−SeNPs size at different GLP concentrations at 24 h; growth inhibition of U87 and C6 cells after exposure to GLP−SeNPs, SeNPs, and GLP for 72 h; viability of different concentrations of GLP−SeNPs on U87 and C6 cells for 24, 48, and 72 h; and intracellular ROS were detected by DHE fluorescence intensity after C6 cells were treated with GLP−SeNPs at different concentrations for 120 min. This material is available free of charge via the Internet at http://pubs.acs.org.

AUTHOR INFORMATION

Corresponding Authors

*(F.Y.) E-mail: tyoung@jnu.edu.cn.
*(W.Z.) E-mail: tzhwj@jnu.edu.cn.
*(T.C.) Phone: +86 20-85225962; fax: +86 20 85221263; e-mail: felixchentf@gmail.com.

Notes

The authors declare no competing financial interest.

ACKNOWLEDGMENTS

This work was financially supported by National High Technology Research and Development Program of China (863 Program, SS2014AA020538), Natural Science Foundation of China and Guangdong Province, Science Foundation for Distinguished Young Scholars of Guangdong Province, Program for New Century Excellent Talents in University, Yang Fan Innovative & Entrepreneurial Research Team Project, Research Fund for the Doctoral Program of Higher Education of China, and China Postdoctoral Science Foundation.

REFERENCES

(1) Bao, S.; Wu, Q.; McLendon, R. E.; Hao, Y.; Shi, Q.; Hjelmeland, A. B.; Dewhirst, M. W.; Bigner, D. D.; Rich, J. N. Glioma Stem Cells Promote Radioresistance by Preferential Activation of the DNA Damage Response. *Nature* **2006**, *444*, 756−760.
(2) Kwak, S. Y.; Yang, J. S.; Kim, B. Y.; Bae, I. H.; Han, Y. H. Ionizing Radiation-Inducible MiR-494 Promotes Glioma Cell Invasion through EGFR Stabilization by Targeting P190B RhoGAP. *Biochim. Biophys. Acta* **2013**, *1843*, 508−516.
(3) Liu, G.; Shen, H.; Mao, J.; Zhang, L.; Jiang, Z.; Sun, T.; Lan, Q.; Zhang, Z. Transferrin Modified Graphene Oxide for Glioma-Targeted Drug Delivery: In Vitro and in Vivo Evaluations. *ACS Appl. Mater. Interfaces* **2013**, *5*, 6909−6914.
(4) Mohme, M.; Neidert, M. C.; Regli, L.; Weller, M.; Martin, R. Immunological Challenges for Peptide-Based Immunotherapy in Glioblastoma. *Cancer Treat. Rev.* **2014**, *40*, 248−258.
(5) Johnson, L. A.; Sampson, J. H. Immunotherapy Approaches for Malignant Glioma from 2007 to 2009. *Curr. Neurol. Neurosci. Rep.* **2010**, *10*, 259−266.
(6) Gu, G.; Gao, X.; Hu, Q.; Kang, T.; Liu, Z.; Jiang, M.; Miao, D.; Song, Q.; Yao, L.; Tu, Y.; Pang, Z.; Chen, H.; Jiang, X.; Chen, J. The Influence of the Penetrating Peptide IRGD on the Effect of Paclitaxel-Loaded MT1-AF7p-Conjugated Nanoparticles on Glioma Cells. *Biomaterials* **2013**, *34*, 5138−5148.
(7) Lawson, H. C.; Sampath, P.; Bohan, E.; Park, M. C.; Hussain, N.; Olivi, A.; Weingart, J.; Kleinberg, L.; Brem, H. Interstitial Chemotherapy for Malignant Gliomas: The Johns Hopkins Experience. *J. Neuro-Oncol.* **2007**, *83*, 61−70.
(8) Squatrito, M.; Holland, E. C. DNA Damage Response and Growth Factor Signaling Pathways in Gliomagenesis and Therapeutic Resistance. *Cancer Res.* **2011**, *71*, 5945−5949.
(9) Gao, H.; Qian, J.; Cao, S.; Yang, Z.; Pang, Z.; Pan, S.; Fan, L.; Xi, Z.; Jiang, X.; Zhang, Q. Precise Glioma Targeting of and Penetration by Aptamer and Peptide Dual-Functioned Nanoparticles. *Biomaterials* **2012**, *33*, 5115−5123.
(10) Xin, H.; Sha, X.; Jiang, X.; Zhang, W.; Chen, L.; Fang, X. Anti-glioblastoma Efficacy and Safety of Paclitaxel-Loading Angiopep-Conjugated Dual Targeting PEG-PCL Nanoparticles. *Biomaterials* **2012**, *33*, 8167−8176.
(11) Sun, X.; Pang, Z.; Ye, H.; Qiu, B.; Guo, L.; Li, J.; Ren, J.; Qian, Y.; Zhang, Q.; Chen, J. Co-delivery of PEGFP-HTRAIL and Paclitaxel to Brain Glioma Mediated by an Angiopep-Conjugated Liposome. *Biomaterials* **2012**, *33*, 916−924.
(12) Jiang, X.; Xin, H.; Ren, Q.; Gu, J.; Zhu, L.; Du, F.; Feng, C.; Xie, Y.; Sha, X.; Fang, X. Nanoparticles of 2-Deoxy-D-glucose Functionalized Poly(ethylene glycol)-co-poly(trimethylene carbonate) for Dual-Targeted Drug Delivery in Glioma Treatment. *Biomaterials* **2014**, *35*, 518−529.
(13) Guo, J.; Gao, X.; Su, L.; Xia, H.; Gu, G.; Pang, Z.; Jiang, X.; Yao, L.; Chen, J.; Chen, H. Aptamer-Functionalized PEG−PLGA Nano-

particles for Enhanced Anti-glioma Drug Delivery. *Biomaterials* **2011**, *32*, 8010−8020.
(14) Rayman, M. P. Selenium in Cancer Prevention: A Review of the Evidence and Mechanism of Action. *Proc. Nutr. Soc.* **2005**, *64*, 527−542.
(15) Wang, H.; Wei, W.; Zhang, S. Y.; Shen, Y. X.; Yue, L.; Wang, N. P.; Xu, S. Y. Melatonin-Selenium Nanoparticles Inhibit Oxidative Stress and Protect against Hepatic Injury Induced by Bacillus Calmette−Guérin/Lipopolysaccharide in Mice. *J. Pineal Res.* **2005**, *39*, 156−163.
(16) Gao, X.; Zhang, J.; Zhang, L. Hollow Sphere Selenium Nanoparticles: Their in-Vitro Anti Hydroxyl Radical Effect. *Adv. Mater.* **2002**, *14*, 290−293.
(17) Huang, Y.; He, L.; Liu, W.; Fan, C.; Zheng, W.; Wong, Y. S.; Chen, T. Selective Cellular Uptake and Induction of Apoptosis of Cancer-Targeted Selenium Nanoparticles. *Biomaterials* **2013**, *34*, 7106−7116.
(18) Sarmento, B.; Ribeiro, A.; Veiga, F.; Ferreira, D. Development and Characterization of New Insulin Containing Polysaccharide Nanoparticles. *Colloids Surf., B* **2006**, *53*, 193−202.
(19) Crini, G. Recent Developments in Polysaccharide-Based Materials Used as Adsorbents in Wastewater Treatment. *Prog. Polym. Sci.* **2005**, *30*, 38−70.
(20) Chen, T.; Xu, S.; Zhao, T.; Zhu, L.; Wei, D.; Li, Y.; Zhang, H.; Zhao, C. Gold Nanocluster-Conjugated Amphiphilic Block Copolymer for Tumor-Targeted Drug Delivery. *ACS Appl. Mater. Interfaces* **2012**, *4*, 5766−5774.
(21) Bowman, K.; Leong, K. W. Chitosan Nanoparticles for Oral Drug and Gene Delivery. *Int. J. Nanomed.* **2006**, *1*, 117−128.
(22) Gan, Q.; Wang, T.; Cochrane, C.; McCarron, P. Modulation of Surface Charge, Particle Size and Morphological Properties of Chitosan−TPP Nanoparticles Intended for Gene Delivery. *Colloids Surf., B* **2005**, *44*, 65−73.
(23) De Campos, A. M.; Sánchez, A.; Alonso, M. a. J. Chitosan Nanoparticles: A New Vehicle for the Improvement of the Delivery of Drugs to the Ocular Surface. Application to Cyclosporin A. *Int. J. Pharm.* **2001**, *224*, 159−168.
(24) Yang, L.; Wang, Y.; Zhou, Q.; Chen, P.; Wang, Y.; Wang, Y.; Liu, T.; Xie, L. Inhibitory Effects of Polysaccharide Extract from Spirulina Platensis on Corneal Neovascularization. *Mol. Vision* **2009**, *15*, 1951−1961.
(25) Chen, M.-Z.; Xie, H.-G.; Yang, L.-W.; Liao, Z.-H.; Yu, J. In Vitro Anti-influenza Virus Activities of Sulfated Polysaccharide Fractions from Gracilaria Lemaneiformis. *Virol. Sin.* **2010**, *25*, 341−351.
(26) Yu, J.; Wang, X.; Chen, M.-Z.; Zhang, Y.-Y.; Long, Z.-J. Analysis on Nutritional Components and Polysaccharide Composition of Gracilaria Lemaneiformis from Chaoshan Coast. *J. Food Sci.* **2006**, *1*, 93−96.
(27) Liu, S.; Liu, Z.; Chen, K.; Yan, Y.; Watzlowik, P.; Wester, H.-J.; Chin, F. T.; Chen, X. 18F-Labeled Galacto and PEGylated RGD Dimers for PET Imaging of $\alpha v\beta 3$ Integrin Expression. *Mol. Imaging Biol.* **2010**, *12*, 530−538.
(28) Yang, W.-G.; Xie, G.-H.; Xu, D.-L.; Zhu, Q.-L.; Lu, J.-F.; Zhou, X.-Y. Degradation of Gracilaria Lemaneiformis Polysaccharide and Antioxidation of Its Degraded Products. *J. Fish. China* **2009**, *2*, 342−347.
(29) Wu, H.; Li, X.; Liu, W.; Chen, T.; Li, Y.; Zheng, W.; Man, C. W.-Y.; Wong, M.-K.; Wong, K.-H. Surface Decoration of Selenium Nanoparticles by Mushroom Polysaccharides−Protein Complexes to Achieve Enhanced Cellular Uptake and Antiproliferative Activity. *J. Mater. Chem.* **2012**, *22*, 9602−9610.
(30) Li, Y.; Li, X.; Wong, Y. S.; Chen, T.; Zhang, H.; Liu, C.; Zheng, W. The Reversal of Cisplatin-Induced Nephrotoxicity by Selenium Nanoparticles Functionalized with 11-Mercapto-1-undecanol by Inhibition of ROS-Mediated Apoptosis. *Biomaterials* **2011**, *32*, 9068−9076.
(31) Nogueira, D. R.; Tavano, L.; Mitjans, M.; Perez, L.; Infante, M. R.; Vinardell, M. P. In Vitro Antitumor Activity of Methotrexate via pH-Sensitive Chitosan Nanoparticles. *Biomaterials* **2013**, *34*, 2758−2772.
(32) Liu, W.; Li, X.; Wong, Y.-S.; Zheng, W.; Zhang, Y.; Cao, W.; Chen, T. Selenium Nanoparticles as a Carrier of 5-Fluorouracil to Achieve Anticancer Synergism. *ACS Nano* **2012**, *6*, 6578−6591.
(33) Fan, Y.; Wang, W.; Song, W.; Chen, H.; Teng, A.; Liu, A. Partial Characterization and Anti-tumor Activity of an Acidic Polysaccharide from *Gracilaria lemaneiformis*. *Carbohydr. Polym.* **2012**, *88*, 1313−1318.
(34) Raveendran, S.; Palaninathan, V.; Chauhan, N.; Sakamoto, Y.; Yoshida, Y.; Maekawa, T.; Mohanan, P. V.; Kumar, D. S. In Vitro Evaluation of Antioxidant Defense Mechanism and Hemocompatibility of Mauran. *Carbohydr. Polym.* **2013**, *98*, 108−115.
(35) Venkatesan, P.; Puvvada, N.; Dash, R.; Prashanth Kumar, B. N.; Sarkar, D.; Azab, B.; Pathak, A.; Kundu, S. C.; Fisher, P. B.; Mandal, M. The Potential of Celecoxib-Loaded Hydroxyapatite-Chitosan Nanocomposite for the Treatment of Colon Cancer. *Biomaterials* **2011**, *32*, 3794−806.
(36) Farokhzad, O. C.; Langer, R. Impact of Nanotechnology on Drug Delivery. *ACS Nano* **2009**, *3*, 16−20.
(37) Lee, M. H.; Kim, J. Y.; Han, J. H.; Bhuniya, S.; Sessler, J. L.; Kang, C.; Kim, J. S. Direct Fluorescence Monitoring of the Delivery and Cellular Uptake of a Cancer-Targeted RGD Peptide-Appended Naphthalimide Theragnostic Prodrug. *J. Am. Chem. Soc.* **2012**, *134*, 12668−12674.
(38) Yu, B.; Zhang, Y.; Zheng, W.; Fan, C.; Chen, T. Positive Surface Charge Enhances Selective Cellular Uptake and Anticancer Efficacy of Selenium Nanoparticles. *Inorg. Chem.* **2012**, *51*, 8956−8963.
(39) Kim, G.; Kim, W.; Kim, K.; Lee, J. DNA Damage and Mitochondria Dysfunction in Cell Apoptosis Induced by Nonthermal Air Plasma. *Appl. Phys. Lett.* **2010**, *96*, 021502.
(40) Sinha, R.; El-Bayoumy, K. Apoptosis Is a Critical Cellular Event in Cancer Chemoprevention and Chemotherapy by Selenium Compounds. *Curr. Cancer Drug Targets* **2004**, *4*, 13−28.
(41) Li, J.; Li, X.; Shi, X.; He, X.; Wei, W.; Ma, N.; Chen, H. Highly Sensitive Detection of Caspase-3 Activities via a Nonconjugated Gold Nanoparticle-Quantum Dot Pair Mediated by an Inner-Filter Effect. *ACS Appl. Mater. Interfaces* **2013**, *5*, 9798−9802.
(42) Wang, Y.-B.; Qin, J.; Zheng, X.-Y.; Bai, Y.; Yang, K.; Xie, L.-P. Diallyl Trisulfide Induces Bcl-2 and Caspase-3-Dependent Apoptosis via Downregulation of Akt Phosphorylation in Human T24 Bladder Cancer Cells. *Phytomedicine* **2010**, *17*, 363−368.
(43) Kantari, C.; Walczak, H. Caspase-8 and Bid: Caught in the Act between Death Receptors and Mitochondria. *Biochim. Biophys. Acta, Mol. Cell Res.* **2011**, *1813*, 558−563.
(44) Li, W. J.; Zhou, J.; Li, B.; Wang, H.; Peng, Y. B.; Wang, Z. PARP Inhibition Restores Erectile Function by Suppressing Corporal Smooth Muscle Apoptosis in Diabetic rats. *J. Sex. Med.* **2011**, *8*, 1072−1082.
(45) Ott, M.; Gogvadze, V.; Orrenius, S.; Zhivotovsky, B. Mitochondria, Oxidative Stress and Cell Death. *Apoptosis* **2007**, *12*, 913−922.
(46) Kang, J. M.; Kim, N.; Kim, J.-H.; Oh, E.; Lee, B.-Y.; Lee, B. H.; Shin, C. M.; Park, J. H.; Lee, M. K.; Nam, R. H. Effect of Aging on Gastric Mucosal Defense Mechanisms: ROS, Apoptosis, Angiogenesis, and Sensory Neurons. *Am. J. Physiol.: Gastrointest. Liver Physiol.* **2010**, *299*, G1147−G1153.
(47) Irani, K. Oxidant Signaling in Vascular Cell Growth, Death, and Survival: A Review of the Roles of Reactive Oxygen Species in Smooth Muscle and Endothelial Cell Mitogenic and Apoptotic Signaling. *Circ. Res.* **2000**, *87*, 179−183.
(48) Speidel, D. Transcription-Independent P53 Apoptosis: An Alternative Route to Death. *Trends Cell Biol.* **2010**, *20*, 14−24.
(49) Liu, C. L.; Tam, J. C.; Sanders, A. J.; Ko, C. H.; Fung, K. P.; Leung, P. C.; Harding, K. G.; Jiang, W. G.; Lau, C. B. Molecular Angiogenic Events of a Two-Herb Wound Healing Formula Involving MAPK and Akt Signaling Pathways in Human Vascular Endothelial Cells. *Wound Repair Regener.* **2013**, *21*, 579−587.

(50) Carracedo, A.; Ma, L.; Teruya-Feldstein, J.; Rojo, F.; Salmena, L.; Alimonti, A.; Egia, A.; Sasaki, A. T.; Thomas, G.; Kozma, S. C. Inhibition of MTORC1 Leads to MAPK Pathway Activation through a PI3K-Dependent Feedback Loop in Human Cancer. *J. Clin. Invest.* **2008**, *118*, 3065−3074.
(51) Altomare, D. A.; Testa, J. R. Perturbations of the AKT Signaling Pathway in Human Cancer. *Oncogene* **2005**, *24*, 7455−7464.